mathematics

MDPI

Article

The Solid–Liquid Phase Interface Dynamics in an Undercooled Melt with a Solid Wall

Ekaterina A. Titova and Dmitri V. Alexandrov *

Laboratory of Multi-Scale Mathematical Modeling, Department of Theoretical and Mathematical Physics, Ural Federal University, Lenin Ave., 51, Ekaterinburg 620000, Russia; eatitova@urfu.ru
* Correspondence: dmitri.alexandrov@urfu.ru

Abstract: A new boundary integral equation for the interface function of a curved solid/liquid phase interface propagating into an undercooled one-component melt is derived in the presence of a solid wall in liquid. Green's function technique is used to transform a purely thermal boundary value problem to a single integro-differential equation for the interface function in two- and three-dimensional cases. It is shown that a solid wall represents an additional source of heat and melt undercooling can be negative in the vicinity of the wall. The new boundary integral equation has a limiting transition to previously developed theory in the absence of a solid wall.

Keywords: boundary integral equation; Green's function technique; phase transitions; propagation of curved solid–liquid interfaces; undercooled melts; dendrites

MSC: 82C26

1. Introduction

Directional and volumetric crystallization are the basis of many technological solidification processes and are often found in nature (e.g., freezing of water and various solutions, solidification of magma) [1–7]. Mathematical models of such processes are based on the description of heat and mass transfer in solid and liquid phases separated by a moving crystallization front. This interphase boundary is generally curvilinear and moves according to a certain time-dependent law, which is determined by solving the problem. The mathematical model of a purely thermal problem was first formulated by Josef Stephan [8–11], and all problems with a moving boundary of phase transformation now bear his name. Note that, in general, the unsteady Stefan problem has no exact analytical solution, and the solution of each individual model strongly depends on the geometry of the crystallization domain and boundary conditions. The solution to such problems is usually constructed using approximate analytical (e.g., the method of differential series [12,13]) and numerical (e.g., the method of fixed boundaries [14]) methods.

One of the fruitful approaches to solving the Stefan problem is the method of boundary integral equation (BIE), first proposed by Nash and Glicksman [15,16]. The idea of this method is to derive an integro-differential equation for the interface function determining the position and velocity of the crystallization front. Note that such an equation was derived in [15,16] for a purely thermal problem. The BIE that describes the thermal concentration problem was derived by Alexandrov and Galenko [17] in the case of parabolic mass transfer in the melt/solution. Further, they considered the scenario of local non-equilibrium (fast) crystallization described by a hyperbolic impurity diffusion equation and derived the corresponding BIE [18]. Note that the high-speed BIE has a limiting transition to the low-speed BIE [18]. An important step in the BIE theory was the case of convective fluid flows considered in [19,20]. Note that the BIE allows us to study the morphological stability of interfacial boundaries of a certain shape [21–23], derive the selection criterion of stable

check for updates

Citation: Titova E.A.; Alexandrov, D.V. The Solid–Liquid Phase Interface Dynamics in an Undercooled Melt with a Solid Wall. *Mathematics* **2024**, *12*, 327. https://doi.org/10.3390/math12020327

Academic Editor: Vasily Novozhilov

Received: 19 December 2023
Revised: 17 January 2024
Accepted: 18 January 2024
Published: 19 January 2024

Copyright: © 2024 by the authors. Licensee MDPI, Basel, Switzerland. This article is an open access article distributed under the terms and conditions of the Creative Commons Attribution (CC BY) license (https://creativecommons.org/licenses/by/4.0/).

growth mode for dendritic crystals [24–26], as well as study the shape and evolution of various patterns [27].

In this paper, we derive a new BIE for the case when a single-component melt or solution crystallizes under the significant influence of a solid wall in liquid. Examples of such processes are (i) dendritic growth in a mold, (ii) freezing of water in lakes of shallow depth, (iii) and solidification of lava in magma chambers. The new BIE has a limiting transition to the previously developed theory in the absence of a solid wall and is found below for 2D and 3D cases.

2. 2D Boundary Integral Equation

Let us consider the evolution of a curved solid/liquid phase transition boundary in an undercooled one-component liquid in the presence of a solid wall (Figure 1). Below, we assume that the one-component melt is motionless, and the BIE is written out in a reference frame that is moving with a constant (V) toward the liquid phase. Also, we assume that the temperature conductivity coefficient D_T is the same constant in both phases. In addition, the solid wall is smooth and planar; no particle nucleation occurs in the bulk melt or at the solid wall. The temperature field in the solid and liquid phases satisfies the temperature conductivity equation in a reference frame that is moving with a constant velocity (V) [28]

$$D_T \nabla^2 T - \frac{\partial T}{\partial t} + V \frac{\partial T}{\partial z} = 0, \tag{1}$$

where T is the temperature, D_T is the thermal conductivity, t is the time and V is the constant velocity of moving Cartesian coordinate systems x, y, and z fixed on the growing crystal (steady-state growth rate). The boundary conditions at the solid/liquid interface take the form [17,20,22,25]

$$\begin{aligned} T = T_i = T_0 - d_c \mathcal{K} \frac{Q}{c_p} - \tilde{\beta}\left(V + \frac{\partial \zeta}{\partial t}\right), \\ D_T\left(\nabla T_{solid} - \nabla T_{liquid}\right) \cdot d\mathbf{s} = \frac{Q}{c_p}\left(V + \frac{\partial \zeta}{\partial t}\right) d^2x, \end{aligned} \tag{2}$$

where d_c is the anisotropy capillary length, $\mathcal{K}$ is the average interface curvature, Q is the latent heat of crystallization, c_p is the heat capacity, $\tilde{\beta}$ is the kinetic coefficient, T_i is the interfacial temperature, T_0 is the phase transition temperature for a flat crystallization front, $d\mathbf{s}$ is the surface area vector element directed towards the liquid phase, and $\zeta(x,t)$ is the interface function. Let us especially emphasize that $\zeta(x,t)$ represents a curved line in 2D whereas $\zeta(x,y,t)$ is a crystal surface in 3D. Note that the boundary conditions (2) represent the Gibbs–Thomson and heat balance conditions, respectively. The average interface curvature $\mathcal{K}$ in a two-dimensional case is determined as

$$\mathcal{K}(x,t) = -\frac{\partial^2 \zeta / \partial x^2}{\left[1 + (\partial \zeta / \partial x)^2\right]^{3/2}}. \tag{3}$$

Here, we consider how a solid wall $z = z_0$ kept at a fixed temperature

$$T(z_0) = T_1 = \text{const}. \tag{4}$$

influences the boundary integral equation. To do this, we use Green's function $G(\mathbf{p}|\mathbf{p}_1)$ to derive an integro-differential equation for the interface function $\zeta(x,t)$. Green's function satisfies the following equation and boundary condition [28,29]

$$\begin{aligned} \frac{\partial G(\mathbf{p}|\mathbf{p}_1)}{\partial t_1} + D_T \nabla_1^2 G(\mathbf{p}|\mathbf{p}_1) - V \frac{\partial G(\mathbf{p}|\mathbf{p}_1)}{\partial z_1} = -\delta(\mathbf{p} - \mathbf{p}_1), \\ G(x, z_0, t | x_1, z_1, t_1) = 0, \end{aligned} \tag{5}$$

where $\mathbf{p} = (x, z, t)$ and $\mathbf{p}_1 = (x_1, z_1, t_1)$.

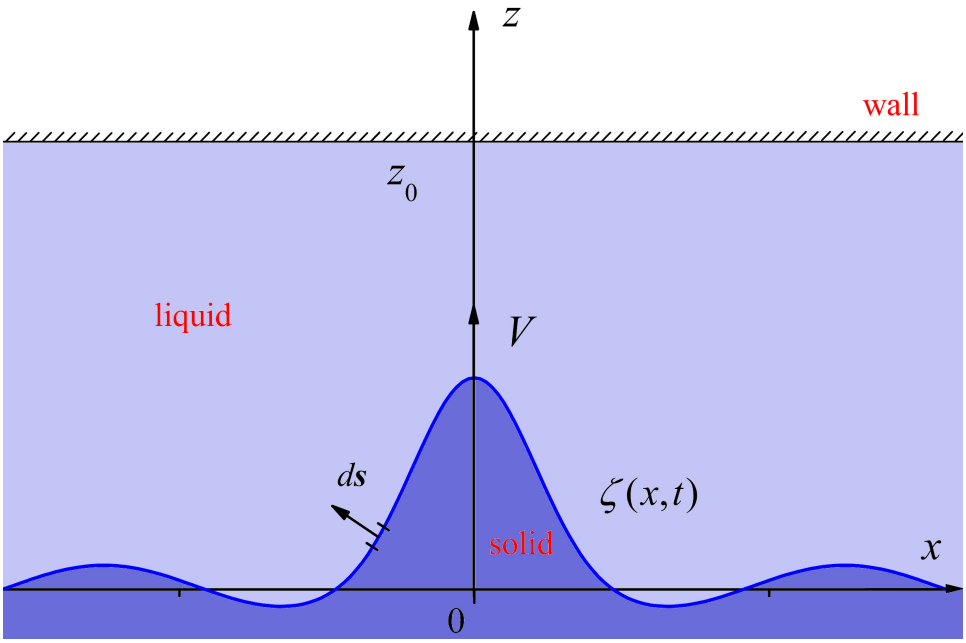

Figure 1. A scheme of solid/liquid interface propagation into an undercooled liquid in the presence of a solid wall $z = z_0$.

Applying the method of images to Green's function for an infinite domain [29], we construct Green's function for the problem under question with a solid wall as follows

$$G(\mathbf{p}|\mathbf{p}_1) = \frac{1}{4\pi D_T(t-t_1)}\left[\exp\left(-\frac{(x-x_1)^2+(z-z_1+V(t-t_1))^2}{4D_T(t-t_1)}\right)\right.$$
$$\left.-\exp\left(-\frac{(x-x_1)^2+(z-2z_0+z_1-V(t-t_1))^2}{4D_T(t-t_1)}\right)\right]. \tag{6}$$

It is easily seen that Green's function (6) satisfies the boundary value problem (5). Note that the first term in expression (6) coincides with Green's function for the unbounded problem [30] (when a solid wall is absent).

Next, multiplying Equation (1) taken at point $\mathbf{p}_1$ by $G(\mathbf{p}|\mathbf{p}_1)$ and then subtracting Equation (5) multiplied by $T(p_1)$, we obtain

$$D_T\Big(G(\mathbf{p}|\mathbf{p}_1)\nabla_1^2 T - T(\mathbf{p}_1)\nabla_1^2 G(\mathbf{p}|\mathbf{p}_1)\Big) - G(\mathbf{p}|\mathbf{p}_1)\frac{\partial T}{\partial t_1} - T(\mathbf{p}_1)\frac{\partial G(\mathbf{p}|\mathbf{p}_1)}{\partial t_1}$$
$$+V\left(G(\mathbf{p}|\mathbf{p}_1)\frac{\partial T}{\partial z_1} + T(\mathbf{p}_1)\frac{\partial G}{\partial z_1}\right) = \delta(\mathbf{p}-\mathbf{p}_1)T(\mathbf{p}_1). \tag{7}$$

Now, we integrate Equation (7) over time and volume

$$D_T\int_{-\infty}^{t+\varepsilon}\int_{\Lambda_1}\Big(G(\mathbf{p}|\mathbf{p}_1)\nabla_1^2 T - T(\mathbf{p}_1)\nabla_1^2 G(\mathbf{p}|\mathbf{p}_1)\Big)dt_1dx_1dz_1$$
$$-\int_{\Lambda_1} G(\mathbf{p}|\mathbf{p}_1)T(\mathbf{p}_1)|_{t_1\to -\infty}^{t_1\to t+\varepsilon}dx_1dz_1 + V\int_{-\infty}^{t+\varepsilon}\int_{-\infty}^{\infty} G(\mathbf{p}|\mathbf{p}_1)T(\mathbf{p}_1)|_{z_1\to -\infty}^{z_1\to z_0}dx_1dt_1 = T(\mathbf{p}), \tag{8}$$

where $\varepsilon > 0$ is an infinitely small parameter and Λ_1 is an integration domain without the interface $\zeta(x,t)$ $(-\infty < x_1 < \infty, -\infty < z_1 < z_0)$.

The second integral in Equation (8) vanishes since Equation (6) gives zero in the limit $t_1 \to -\infty$, and $G(\mathbf{p}|\mathbf{p}_1) = 0$ when $t_1 > t$ (causality condition). Considering the third

integral in (8) with allowance for $T(z_1 \to z_0) = T_1 = \text{const.}$ and $T(z_1 \to -\infty) = \text{const.}$, we are able to integrate Green's function as follows

$$V \int_{-\infty}^{t+\varepsilon} \int_{-\infty}^{\infty} G(\mathbf{p}|\mathbf{p}_1) dx_1 dt_1 = \begin{cases} \exp\left((z_1 - z)\dfrac{V}{D_T}\right), & z > z_1, \\ 1, & z < z_1. \end{cases} - \begin{cases} \exp\left((z_1 + z - 2z_0)\dfrac{V}{D_T}\right), & z - 2z_0 + z_1 < 0, \\ 1, & z - 2z_0 + z_1 > 0. \end{cases} \tag{9}$$

Here, the coordinate $z_1 \in (z_0, -\infty)$. At $z_1 \to -\infty$, both terms on the right-hand side of expression (9) are vanishing. Considering the boundary $z_1 = z_0$ and taking into account that the total domain of the problem under question is bounded by the solid wall, we arrive at

$$V \int_{-\infty}^{t+\varepsilon} \int_{-\infty}^{\infty} G(\mathbf{p}|\mathbf{p}_1) T(\mathbf{p}_1)|_{z_1 \to -\infty}^{z_1 \to z_0} dx_1 dt_1 = T_1 \left(1 - \exp\left((z - z_0)\frac{V}{D_T}\right)\right). \tag{10}$$

Now, we apply Green's second identity to the first term in (8)

$$\begin{aligned} &\int_{-\infty}^{t+\varepsilon} \int_{\Lambda_1} \left(G(\mathbf{p}|\mathbf{p}_1)\nabla_1^2 T - T(\mathbf{p}_1)\nabla_1^2 G(\mathbf{p}|\mathbf{p}_1)\right) dt_1 dx_1 dz_1 \\ &= \int_{-\infty}^{t+\varepsilon} \int_{S_1} \left(G(\mathbf{p}|\mathbf{p}_1)\nabla_1 T - T(\mathbf{p}_1)\nabla_1 G(\mathbf{p}|\mathbf{p}_1)\right) \cdot dS_1 dt_1, \end{aligned} \tag{11}$$

where S_1 is a boundary encompassing the volume Λ_1 in 3D. By substituting (10) and (11) into (8), we have

$$\begin{aligned} D_T \int_{-\infty}^{t+\varepsilon} \int_{S_1} &\left(G(\mathbf{p}|\mathbf{p}_1)\nabla_1 T - T(\mathbf{p}_1)\nabla_1 G(\mathbf{p}|\mathbf{p}_1)\right) \cdot dS_1 dt_1 \\ &+ T_1 \left(1 - \exp\left((z - z_0)\frac{V}{D_T}\right)\right) = T(\mathbf{p}). \end{aligned} \tag{12}$$

The integral containing $\nabla_1 G(\mathbf{p}|\mathbf{p}_1)$ vanishes due to the continuity of temperature T [28,30]. Approaching the point $\mathbf{p}$ to the interface and using the heat balance condition (2), we come to

$$\frac{Q}{c_p} \int_{-\infty}^{t+\varepsilon} \int_{-\infty}^{\infty} G(\mathbf{p}|\mathbf{p}_1) \left(V + \frac{\partial \zeta_1}{\partial t_1}\right) dt_1 dx_1 + T_1 \left(1 - \exp\left((\zeta - z_0)\frac{V}{D_T}\right)\right) = T_i, \tag{13}$$

where $\zeta_1 = \zeta(x_1, t_1)$.

The final step is to use the Gibbs–Thomson condition (2), which gives

$$\begin{aligned} \Delta - d_c \mathcal{K} + T_2 \exp\left((\zeta - z_0)\frac{V}{D_T}\right) - \beta\left(V + \frac{\partial \zeta}{\partial t}\right) \\ = \int_{-\infty}^{t+\varepsilon} \int_{-\infty}^{\infty} G(\mathbf{p}|\mathbf{p}_1) \left(V + \frac{\partial \zeta_1}{\partial t_1}\right) dt_1 dx_1. \end{aligned} \tag{14}$$

Here, Green's function $G(\mathbf{p}|\mathbf{p}_1)$ is defined by expression (6), $\beta = \tilde{\beta}c_p/Q$ and we introduce the dimensionless undercooling $\Delta = (T_0 - T_1)c_p/Q$ and temperature $T_2 = T_1c_p/Q$. Note that Equation (14) transforms to the corresponding BIE in the case of an unbounded domain at $z_0 \to \infty$, i.e., (see, among others, [15,30])

$$\Delta - d_c\mathcal{K} - \beta\left(V + \frac{\partial\zeta}{\partial t}\right) = \frac{1}{4\pi D_T}\int\limits_{-\infty}^{t+\varepsilon}\int\limits_{-\infty}^{\infty}\frac{1}{t-t_1}\exp\left(-\frac{(x-x_1)^2 + (\zeta - \zeta_1 + V(t-t_1))^2}{4D_T(t-t_1)}\right)\left(V + \frac{\partial\zeta_1}{\partial t_1}\right)dt_1dx_1. \tag{15}$$

As a special note, Equation (15) has a particular solution for a parabolic/paraboloidal dendrite previously discussed by Brener and Mel'nikov [25]. These dendritic shapes are the exact solutions of the BIE (15) in 2D and 3D cases when the interface curvature $\mathcal{K}$ is negligible or constant.

3. 2D Stationary Crystallization

Let us write the BIE (14) in dimensionless coordinates, where the dendrite tip diameter ρ plays the role of the length scale, and z_0, ζ, and x (ζ_1 and x_1) are now dimensionless (for the sake of simplicity, we use here the same designations). In addition, we use the dimensionless time and spatial coordinates in the BIE with time scale ρ/V. As a result, we have

$$\begin{aligned}\Delta - \frac{d_c}{\rho}\mathcal{K} + T_2\exp((\zeta - z_0)2P_T) - \beta V\left(1 + \frac{\partial\zeta}{\partial t}\right) &= \frac{P_T}{2\pi}\int\limits_0^{\infty}\int\limits_{-\infty}^{\infty}\exp\left(-\frac{P_T}{2\tau}(x-x_1)^2\right)\left[\exp\left(-\frac{P_T}{2\tau}(\zeta - \zeta_1 + \tau)^2\right)\right.\\ \left.-\exp\left(-\frac{P_T}{2\tau}(\zeta - 2z_0 + \zeta_1 - \tau)^2\right)\right]\left(1 + \frac{\partial\zeta_1(x_1, t-\tau)}{\partial t}\right)\frac{d\tau}{\tau}dx_1.\end{aligned} \tag{16}$$

Here, $\tau = t - t_1$ and $P_T = \rho V/(2D_T)$ is the Péclet number. Let us consider the frequently occurring case of steady-state crystal growth with a constant velocity. Under such conditions, the interface function $\zeta = \zeta(x)$ does not depend on time and the BIE (16) transforms to

$$\begin{aligned}\Delta - \frac{d_c}{\rho}\mathcal{K} + T_2\exp((\zeta - z_0)2P_T) - \beta V &= \frac{P_T}{2\pi}\\ \times\left[\int\limits_{-\infty}^{\infty}dx_1\exp(P_T(\zeta_1 - \zeta))\int\limits_0^{\infty}\frac{d\tau}{\tau}\exp\left(-\frac{P_T}{2}\left(\frac{(x-x_1)^2 + (\zeta - \zeta_1)^2}{\tau} + \tau\right)\right)\right.\\ \left.-\int\limits_{-\infty}^{\infty}dx_1\exp(P_T(\zeta_1 + \zeta_0))\int\limits_0^{\infty}\frac{d\tau}{\tau}\exp\left(-\frac{P_T}{2}\left(\frac{(x-x_1)^2 + (\zeta_0 + \zeta_1)^2}{\tau} + \tau\right)\right)\right]\end{aligned} \tag{17}$$

with $\zeta_0 = \zeta - 2z_0$. Replacing the variable τ in (17) by y_1 and y_2

$$\frac{\tau}{\sqrt{(x-x_1)^2 + (\zeta - \zeta_1)^2}} = y_1, \quad \frac{\tau}{\sqrt{(x-x_1)^2 + (\zeta_0 + \zeta_1)^2}} = y_2, \tag{18}$$

and taking into account that the integrals over y_1 and y_2 are even functions, we obtain

$$\Delta - \frac{d_c}{\rho}\mathcal{K} + T_2 \exp((\zeta - z_0)2P_T) - \beta V = \frac{P_T}{\pi} \times \left[\int_{-\infty}^{\infty} dx_1 \exp(P_T(\zeta_1 - \zeta)) \int_0^{\infty} dy_1 \exp\left(-\frac{P_T}{2}\sqrt{(x-x_1)^2 + (\zeta - \zeta_1)^2}\left(e^{y_1} + e^{-y_1}\right)\right) - \int_{-\infty}^{\infty} dx_1 \exp(P_T(\zeta_1 + \zeta_0)) \int_0^{\infty} dy_2 \exp\left(-\frac{P_T}{2}\sqrt{(x-x_1)^2 + (\zeta_0 + \zeta_1)^2}\left(e^{y_2} + e^{-y_2}\right)\right)\right]. \quad (19)$$

By using the definition of the modified Bessel function, we now come to the BIE describing the steady-state crystal growth

$$\Delta - \frac{d_c}{\rho}\mathcal{K} + T_2 \exp((\zeta - z_0)2P_T) - \beta V = \frac{P_T}{\pi} \times \left[\int_{-\infty}^{\infty} dx_1 \exp(P_T(\zeta_1 - \zeta)) K_0\left(-P_T\sqrt{(x-x_1)^2 + (\zeta - \zeta_1)^2}\right) - \int_{-\infty}^{\infty} dx_1 \exp(P_T(\zeta_1 + \zeta_0)) K_0\left(-P_T\sqrt{(x-x_1)^2 + (\zeta_0 + \zeta_1)^2}\right)\right]. \quad (20)$$

4. Parabolic Dendrite

As a special case, we consider the growth of a parabolic dendrite with the dimensionless interface function

$$\zeta = -\frac{x^2}{2}, \quad \zeta_1 = -\frac{x_1^2}{2}, \quad (21)$$

Substituting the interface function (21) into the BIE (14) and integrating Green's function over the unbounded region, we have

$$\Delta - \frac{d_c\mathcal{K}}{\rho} + T_2 \exp\left(-P_T(x^2 + 2z_0)\right) - \beta V = \sqrt{\pi P_T}\exp(P_T)\mathrm{erfc}(\sqrt{P_T}) - \int_0^{\infty}\int_{-\infty}^{\infty} \frac{P_T}{2\pi\tau}\exp\left(-\frac{P_T}{2\tau}\left((x-x_1)^2 + \left(2z_0 + \frac{x^2 + x_1^2}{2} + \tau\right)^2\right)\right) d\tau dx_1. \quad (22)$$

Figures 2 and 3 show the melt undercooling determined by Equation (22). As can be seen, the wall represents an additional source of heat and the undercooling can be negative at small distances from the wall. In this case, we have melting instead of crystallization. It should be emphasized that melt undercooling depends only on the Péclet number if there is no solid wall and if interface curvature is constant or negligible. Contrary to this, melt undercooling is a function of both the Péclet number and the distance between the crystal and the solid wall in a semi-bounded problem. In addition, this distance depends on the x-coordinate. It means that the interface temperature and melt undercooling are also dependent on x.

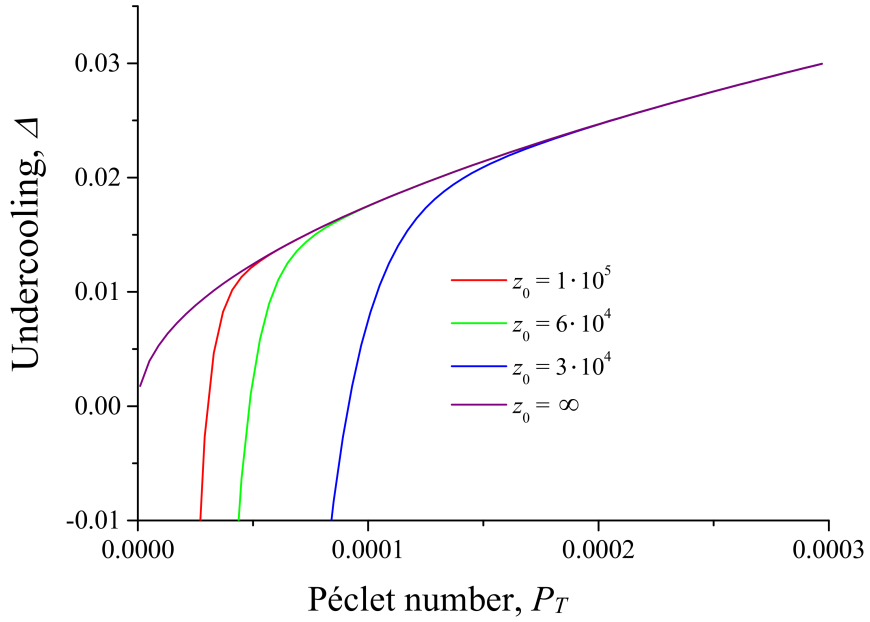

Figure 2. Undercooling at different distances from the flat wall, $x = 0$, $T_1 = 1680$ K, $\beta = d_c = 0$.

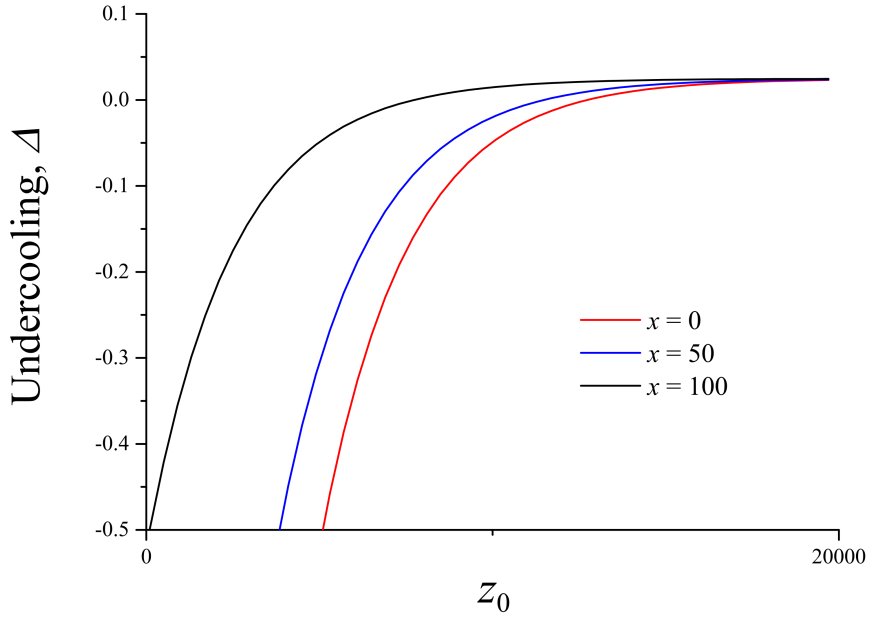

Figure 3. Undercooling at different distances from the flat wall at fixed $P_T = 2 \times 10^{-4}$, $T_1 = 1680$ K, $\beta = d_c = 0$.

5. 3D Boundary Integral Equation

Here, we consider a more general and realistic case of the three-dimensional problem defined by Equations (1), (2), and (4). Green's function for the 3D problem reads as

$$G_{3D}(\mathbf{p}|\mathbf{p}_1) = \left(\frac{D_T}{\pi V^2 (t-t_1)}\right)^{3/2} \left[\exp\left(-\frac{|\mathbf{x}-\mathbf{x}_1|^2 + (z - z_1 + V(t-t_1))^2}{4D_T(t-t_1)}\right) - \exp\left(-\frac{|\mathbf{x}-\mathbf{x}_1|^2 + (z - 2z_0 + z_1 - V(t-t_1))^2}{4D_T(t-t_1)}\right)\right]. \quad (23)$$

Here, $\mathbf{p} = (x, y, z, t)$, $\mathbf{p}_1 = (x_1, y_1, z_1, t_1)$, $\mathbf{x} = (x, y)$, and $\mathbf{x}_1 = (x_1, y_1)$. The 3D boundary integral equation can be obtained by analogy with the 2D case. In dimensionless coordinates, it takes the form of

$$\begin{aligned} &\Delta - \frac{d_c}{\rho}\mathcal{K} + T_2 \exp((\zeta - 2z_0)P_T) - \beta V\left(1 + \frac{\partial \zeta}{\partial t}\right) \\ &= \left(\frac{P_T}{2\pi}\right)^{3/2} \int_0^\infty \frac{d\tau}{\tau^{3/2}} \int_{-\infty}^{\infty}\int_{-\infty}^{\infty} \left[\exp\left(-\frac{P_T}{2\tau}\left[|\mathbf{x} - \mathbf{x}_1|^2 + (\zeta - \zeta_1 + \tau)^2\right)\right]\right. \\ &\left. - \exp\left(-\frac{P_T}{2\tau}\left[|\mathbf{x} - \mathbf{x}_1|^2 + (\zeta - 2z_0 + \zeta_1 - \tau)^2\right]\right)\left(1 + \frac{\partial \zeta_1}{\partial t_1}\right)\right] dx_1 dy_1. \end{aligned} \tag{24}$$

6. Paraboloid of Revolution

The steady-state growth of a needle 3D dendrite can be modeled by the BIE with a paraboloid of revolution as an interface function

$$\zeta = -\frac{x^2 + y^2}{2}, \quad \zeta_1 = -\frac{x_1^2 + y_1^2}{2}. \tag{25}$$

In the dimensionless time and spatial coordinates defined in Section 4, the BIE (14) for the phase transition interface (25) transforms to

$$\begin{aligned} &\Delta - \frac{d_c\mathcal{K}}{\rho} + T_2 \exp\left(-P_T(x^2 + y^2 + 2z_0)\right) - \beta V \\ &= P_T \exp(P_T) \int_1^\infty \frac{\exp(-P_T\eta)}{\eta} d\eta - \left(\frac{P_T}{2\pi}\right)^{3/2} \int_0^\infty \frac{d\tau}{\tau^{3/2}} \\ &\times \int_{-\infty}^{\infty}\int_{-\infty}^{\infty} dx_1 dy_1 \exp\left(-\frac{P_T}{2\tau}\left(|\mathbf{x} - \mathbf{x}_1|^2 + \left(2z_0 + \frac{x^2 + y^2 + x_1^2 + y_1^2}{2} + \tau\right)^2\right)\right). \end{aligned} \tag{26}$$

7. Conclusions

In this paper, we derive a new boundary integral equation (BIE) for the interface function describing the motion of an interfacial boundary in a semi-bounded domain of supercooled melt adjacent to a solid wall of constant temperature. Such a temperature regime can be achieved in practice by artificially maintaining a constant temperature at the boundary (e.g., on the walls of an ingot mold, an ice surface, or the bottom of a lava chamber). This new BIE is derived using Green's function technique for both 2D and 3D cases (formulas (14) and (24), respectively). The derived BIE transitions to the previously known theory if we take the distance between the solid/liquid interface and the solid wall to infinity. The new BIE has been analyzed for the growth of a parabolic dendrite. The solution shows that melt undercooling near a solid wall can become negative because such a wall reflects heat. This in turn leads to the melting of the crystal instead of solidification. An important fact is that the total melt undercooling depends on both the Péclet number and the distance between a curved crystal surface and the solid wall. This means that this undercooling is different at different points on the crystal surface. This means that the dendrite tip slows down as it approaches the wall due to a smaller driving force (melt supercooling). Therefore, the dendrite shape (the surface that envelops its tip and secondary branches) becomes wider near a solid wall. If we consider the growth of several dendrites together (the growth of a dendritic forest), a crystal evolving close to a given dendrite can act as a solid wall (heat source). Therefore, the growth of dendritic branches in the corresponding spatial direction will be retarded. This conclusion is confirmed by experimental data and computer simulations of dendritic growth [31], where the near-complete disappearance of secondary branches of neighboring dendrites was recorded.

In summary, the following new results have been obtained:

- A new BIE for a curved solid/liquid interface propagating into a single-component supercooled melt with a solid wall of constant temperature has been derived.
- An analytical solution of this BIE for a parabolic dendrite is obtained. This solution demonstrates that melt undercooling near a solid surface can be negative when the wall reflects heat and melting occurs.
- It has been shown that the solid wall leads to a smaller driving force, which decelerates the dendrite tip motion and enlarges the crystal shape.

It is of interest to generalize this theory to the effect of a curved solid wall or several solid walls in the melt, modeling the real geometry of an ingot mold [32,33]. An important step is also the generalization of the theory for binary melts, where the impurity redistribution upstream of the solid/liquid interface as well as impurity absorption by the solid phase play a decisive role in the crystallization process and the properties of the solidified phase. Since improved properties of materials are often observed at high crystal growth rates, generalization is also required for local nonequilibrium solidification processes with hyperbolic mass transfer in liquid [18,34–39]. The BIE should also be generalized for convective solidification in the presence of a solid wall [19,20,40–43]. The BIE describing the morphology of solid phase protrusions in the two-phase region can also be used to determine the solid phase fraction in this region and, consequently, how the heat and mass transfer coefficient depends on the solid phase fraction. Therefore, it is reasonable to combine the present approach with the two-phase region theory [44–50] for more accurate modeling of the directional solidification process. The influence of these effects is important for studying the dynamics of a curved crystallization front in the presence of a solid wall. For this purpose, it is necessary to use the boundary integral method under consideration (developed in the presence of a solid wall) and the theories of the aforementioned papers (elaborated on in the absence of a solid wall).

Author Contributions: Conceptualization, E.A.T. and D.V.A.; methodology, E.A.T. and D.V.A.; software, E.A.T.; validation, E.A.T. and D.V.A.; formal analysis, E.A.T. and D.V.A.; investigation, E.A.T. and D.V.A.; resources, D.V.A.; writing—original draft preparation, E.A.T. and D.V.A.; writing—review and editing, E.A.T. and D.V.A.; visualization, E.A.T.; supervision, E.A.T. and D.V.A.; project administration, E.A.T. and D.V.A.; funding acquisition, E.A.T. and D.V.A. All authors have read and agreed to the published version of the manuscript.

Funding: This work was financially supported by the Ministry of Science and Higher Education of the Russian Federation (project no. FEUZ-2023-0022).

Data Availability Statement: All data generated or analyzed during this study are included in this published article.

Conflicts of Interest: The authors declare no conflicts of interest.

References

1. Kurz, W.; Fisher, D.J.; Trivedi, R. Progress in modelling solidification microstructures in metals and alloys: Dendrites and cells from 1700 to 2000. *Int. Mater. Rev.* **2019**, *64*, 311–354. [CrossRef]
2. Kurz, W.; Rappaz, M.; Trivedi, R. Progress in modelling solidification microstructures in metals and alloys. Part II: Dendrites from 2001 to 2018. *Int. Mater. Rev.* **2021**, *66*, 30–76. [CrossRef]
3. Worster, M.G. Solidification of an alloy from a cooled boundary. *J. Fluid Mech.* **1986**, *167*, 481–501. [CrossRef]
4. Wettlaufer, J.S.; Worster, M.G.; Huppert, E. The phase evolution of young sea ice. *Geophys. Res.* **1997**, *24*, 1251–1254. [CrossRef]
5. Worster, M.G.; Huppert, H.E.; Sparks, R.S.J. The crystallization of lava lakes. *J. Geophys. Res.* **1993**, *98*, 15891–15901. [CrossRef]
6. Makoveeva, E.V. Steady-state crystallization with a mushy layer: A test of theory with experiments. *Eur. Phys. J. Spec. Top.* **2023**, *232*, 1165–1169. [CrossRef]
7. Herlach, D.; Galenko, P.; Holland-Moritz, D. *Metastable Solids from Undercooled Melts*; Elsevier: Amsterdam, The Netherlands, 2007.
8. Wettlaufer, J.S. The Stefan problem: Polar exploration and the mathematics of moving boundaries. In *Die Zentralanstalt für Meteorologie und Geodynamik, 1851–2001, 150 Jahre Meteorologie und Geophysik in Osterreich*; Styria Verlag: Graz, Austria, 2001; pp. 420–435.
9. Rubinstein, L.I. *The Stefan Problem*; American Mathematical Society: Providence, RI, USA, 1971.
10. Meirmanov, A.M. *The Stefan Problem*; De Gruyter Expositions in Mathematics; De Gruyter: Berlin, Germany, 1992.

11. Alexandrov, D.V.; Ivanov, A.A. The Stefan problem of solidification of ternary systems in the presence of moving phase transition regions. *J. Exper. Theor. Phys.* **2009**, *108*, 821–829 [CrossRef]
12. Lubov, B.Y. *The Theory of Crystallization in Large Volumes*; Nauka: Moscow, Russia, 1975.
13. Alexandrov, D.V. Nucleation and evolution of spherical crystals with allowance for their unsteady-state growth rates. *J. Phys. A Math. Theor.* **2018**, *51*, 075102. [CrossRef]
14. Samarskii, A.A.; Vabishchevich, P.N. *Computational Heat Transfer, Vol.1, Mathematical Modelling*; Wiley: Chichester, UK, 1995.
15. Nash, G.E. Capillary-limited, steady state dendritic growth. Part I. Theoretical development. *NRL Rep.* **1974**, *7679*. Available online: https://apps.dtic.mil/sti/citations/AD0780781 (accessed on 1 December 2023).
16. Nash, G.E.; Glicksman, M.E. Capillary-limited steady-state dendritic growth—I. Theoretical development. *Acta Metall.* **1974**, *22*, 1283–1290. [CrossRef]
17. Alexandrov, D.V.; Galenko, P.K. Boundary integral approach for propagating interfaces in a binary non-isothermal mixture. *Physica A* **2017**, *469*, 420–428. [CrossRef]
18. Alexandrov, D.V.; Galenko, P.K. Selected mode for rapidly growing needle-like dendrite controlled by heat and mass transport. *Acta Mater.* **2017**, *137*, 64–70. [CrossRef]
19. Saville, D.A.; Beaghton, P.J. Growth of needle-shaped crystals in the presence of convection. *Phys. Rev. A* **1988**, *37*, 3423–3430. [CrossRef] [PubMed]
20. Titova, E.A.; Alexandrov, D.V. The boundary integral equation for curved solid/liquid interfaces propagating into a binary liquid with convection. *J. Phys. A Math. Theor.* **2022**, *55*, 055701. [CrossRef]
21. Ben Amar, M.; Pelcé, P. Impurity effect on dendritic growth. *Phys. Rev. A* **1989**, *39*, 4263–4269. [CrossRef] [PubMed]
22. Bouissou, Ph.; Pelcé, P. Effect of a forced flow on dendritic growth. *Phys. Rev. A* **1989**, *40*, 6673–6680. [CrossRef] [PubMed]
23. Alexandrov, D.V.; Galenko, P.K.; Herlach, D.M. Selection criterion for the growing dendritic tip in a non-isothermal binary system under forced convective flow. *J. Cryst. Growth* **2010**, *312*, 2122–2127. [CrossRef]
24. Barbieri, A.; Langer, J.S. Predictions of dendritic growth rates in the linearized solvability theory. *Phys. Rev. A* **1989**, *39*, 5314–5325. [CrossRef]
25. Brener, E.A.; Mel'nikov, V.I. Pattern selection in two-dimensional dendritic growth. *Adv. Phys.* **1991**, *40*, 53–97. [CrossRef]
26. Brener, E.A.; Mel'nikov, V.A. Two-dimensional dendritic growth at arbitrary Peclet number. *J. Phys. Fr.* **1990**, *51*, 157–166. [CrossRef]
27. Pelce, P.; Pomeau, Y. Dendrites in the small undercooling limit. *Stud. Appl. Math.* **1986**, *74*, 245–258. [CrossRef]
28. Langer, J.S. Studies in the theory of interfacial stability—II. Moving symmetric model. *Acta Metall.* **1977**, *25*, 1121–1137. [CrossRef]
29. Morse, P.M.; Feshbach, H. *Methods of Theoretical Physics*; McGraw-Hill: New York, NY, USA, 1953.
30. Langer, J.S.; Turski, L.A. Studies in the theory of interfacial stability—I. Stationary symmetric model. *Acta Metall.* **1977**, *25*, 1113–1119. [CrossRef]
31. Hu, M.; Sun, C.; Fang, H.; Zhu, M. Competitive dendrite growth during directional solidification of a transparent alloy: Modeling and experiment. *Eur. Phys. J. E* **2020**, *43*, 16. [CrossRef] [PubMed]
32. Kermanpur, A.; Eskandari, M.; Purmohamad, H.; Soltani, M.A.; Shateri, R. Influence of mould design on the solidification of heavy forging ingots of low alloy steels by numerical simulation. *Mater. Des.* **2010**, *31*, 1096–1104. [CrossRef]
33. Abootorabi, A.; Korojy, B.; Jabbareh, M.A. Effect of mould design on the Niyama criteria during solidification of CH3C 80t ingot. *Ironmak. Steelmak.* **2019**, *47*, 722–730. [CrossRef]
34. Galenko, P.K.; Danilov, D.A. Local nonequilibrium effect on rapid dendritic growth in a binary alloy melt. *Phys. Lett. A* **1997**, *235*, 271–280. [CrossRef]
35. Galenko, P.K.; Danilov, D.A. Model for free dendritic alloy growth under interfacial and bulk phase nonequilibrium conditions. *J. Cryst. Growth* **1999**, *197*, 992–1002. [CrossRef]
36. Galenko, P.K.; Danilov, D.A. Selection of the thermodynamically stable regime of rapid solidification front motion in an isothermal binary alloy. *J. Cryst. Growth* **2000**, *216*, 512–526. [CrossRef]
37. Zhang, L.; Danilova, E.V.; Steinbach, I.; Medvedev, D.; Galenko, P.K. Diffuse-interface modeling of solute trapping in rapid solidification: Predictions of the hyperbolic phase-field model and parabolic model with finite interface dissipation. *Acta Mater.* **2013**, *61*, 4155–4168. [CrossRef]
38. Lebedev, V.G.; Abramova, E.V.; Danilov, D.A.; Galenko, P.K. Phase-field modeling of solute trapping: Comparative analysis of parabolic and hyperbolic models. *Int. J. Mater. Res.* **2010**, *101*, 473–479. [CrossRef]
39. Kharchenko, D.; Lysenko, I.; Galenko, P.K. Fluctuation effects on pattern selection in the hyperbolic model of phase decomposition. *Stoch. Differ. Equ.* **2011**, *97*, 97–127.
40. Wolff, F.; Viskanta, R. Solidification of a pure metal at a vertical wall in the presence of liquid superheat. *Int. J. Heat Mass Trans.* **1988**, *31*, 1735–1744. [CrossRef]
41. Gau, C.; Viskanta, R.C. Melting and solidification of a pure metal on a vertical wall. *J. Heat Transfer* **1986**, *108*, 174–181. [CrossRef]
42. Galenko, P.K.; Funke, O.; Wang, J.; Herlach, D.M. Kinetics of dendritic growth under the influence of convective flow in solidification of undercooled droplets. *Mater. Sci. Eng. A* **2004**, *375–377*, 488–492. [CrossRef]
43. Roshchupkina, O.; Shevchenko, N.; Eckert, S. Observation of dendritic growth under the influence of forced convection. *IOP Conf. Ser. Mater. Sci. Eng.* **2015**, *84*, 012080. [CrossRef]
44. Huppert, H.E. The fluid mechanics of solidification. *J. Fluid Mech.* **1990**, *212*, 209–240. [CrossRef]

45. Chiareli, A.O.P.; Huppert, H.E.; Worster, M.G. Segregation and flow during the solidification of alloys. *J. Cryst. Growth* **1994**, *139*, 134–146. [CrossRef]
46. Peppin, S.S.L.; Aussillous, P.; Huppert, H.E.; Worster, M.G. Steady-state mushy layers: Experiments and theory. *J. Fluid Mech.* **2007**, *570*, 69–77. [CrossRef]
47. Makoveeva, E.V.; Alexandrov, D.V.; Ivanov, A.A.; Alexandrova, I.V. Desupersaturation dynamics in solutions with applications to bovine and porcine insulin crystallization. *J. Phys. A Math. Theor.* **2023**, *56*, 455702. [CrossRef]
48. Makoveeva, E.V.; Ivanov, A.A. Analysis of an integro-differential model for bulk continuous crystallization with account of impurity feeding, dissolution/growth of nuclei and removal of product crystals. *Math. Meth. Appl. Sci.* **2023**. [CrossRef]
49. Makoveeva, E.V. Mathematical modeling of the crystal growth process in a binary system. *AIP Conf. Proc.* **2020**, *2313*, 030058.
50. Nizovtseva, I.G.; Starodumov, I.O.; Pavlyuk, E.V.; Ivanov, A.A. Mathematical modeling of binary compounds with the presence of a phase transition layer. *Math. Meth. Appl. Sci.* **2021**, *44*, 12260–12270. [CrossRef]

Disclaimer/Publisher's Note: The statements, opinions and data contained in all publications are solely those of the individual author(s) and contributor(s) and not of MDPI and/or the editor(s). MDPI and/or the editor(s) disclaim responsibility for any injury to people or property resulting from any ideas, methods, instructions or products referred to in the content.